

TOPoS: IV. Chemical abundances from high-resolution observations of seven EMP stars[★]

P. Bonifacio¹, E. Caffau¹, M. Spite¹, F. Spite¹, L. Sbordone², L. Monaco³, P. François^{1,4}, B. Plez⁵, P. Molaro⁶, A. J. Gallagher^{7,1}, R. Cayrel¹, N. Christlieb⁸, R. S. Klessen⁹, A. Koch^{10,11}, H.-G. Ludwig^{8,1}, M. Steffen^{12,1}, S. Zaggia¹³, and C. Abate¹⁴

- ¹ GEPI, Observatoire de Paris, PSL Research University, CNRS, Place Jules Janssen, 92190 Meudon, France
- ² European Southern Observatory, Casilla 19001, Santiago, Chile
- ³ Departamento de Ciencias Físicas, Universidad Andres Bello, Fernandez Concha 700, Las Condes, Santiago, Chile
- ⁴ UPJV, Université de Picardie Jules Verne, 33 Rue St Leu, F-80080 Amiens
- ⁵ Laboratoire Univers et Particules de Montpellier, LUPM, Université de Montpellier, CNRS, 34095 Montpellier cedex 5, France
- ⁶ Istituto Nazionale di Astrofisica, Osservatorio Astronomico di Trieste, Via G.B. Tiepolo 11, 34143 Trieste, Italy
- ⁷ Max Planck Institute for Astronomy, Königstuhl 17, 69117 Heidelberg, Germany
- ⁸ Zentrum für Astronomie der Universität Heidelberg, Landessternwarte, Königstuhl 12, 69117 Heidelberg, Germany
- ⁹ Zentrum für Astronomie der Universität Heidelberg, Institut für Theoretische Astrophysik, Albert-Ueberle-Straße 2, 69120 Heidelberg, Germany
- ¹⁰ Zentrum für Astronomie der Universität Heidelberg, Astronomisches Rechen-Institut, Mönchhofstraße 1214, 69120 Heidelberg, Germany
- ¹¹ Department of Physics, Lancaster University, LA1 4YB, Lancaster, UK
- ¹² Leibniz-Institut für Astrophysik Potsdam (AIP), An der Sternwarte 16, 14482 Potsdam, Germany
- ¹³ Istituto Nazionale di Astrofisica, Osservatorio Astronomico di Padova, Vicolo dell'Osservatorio 5, 35122 Padova, Italy
- ¹⁴ Argelander Institut für Astronomie, Auf dem Hügel 71, 53121, Bonn, Germany

Received ...; Accepted ...

ABSTRACT

Context. Extremely metal-poor stars provide us with indirect information on the first generations of massive stars. The TOPoS survey has been designed to increase the census of these stars and to provide a chemical inventory that is as detailed as possible.

Aims. Seven of the most iron-poor stars have been observed with the UVES spectrograph at the ESO VLT Kueyen 8.2 m telescope to refine their chemical composition.

Methods. We analysed the spectra based on 1D LTE model atmospheres, but also used 3D hydrodynamical simulations of stellar atmospheres.

Results. We measured carbon in six of the seven stars: all are carbon-enhanced and belong to the low-carbon band, defined in the TOPoS II paper. We measured lithium ($A(\text{Li})=1.9$) in the most iron-poor star (SDSS J1035+0641, $[\text{Fe}/\text{H}] < -5.2$). We were also able to measure Li in three stars at $[\text{Fe}/\text{H}] \sim -4.0$, two of which lie on the Spite plateau.

We confirm that SDSS J1349+1407 is extremely rich in Mg, but not in Ca.

It is also very rich in Na. Several of our stars are characterised by low α -to-iron ratios.

Conclusions. The lack of high-carbon band stars at low metallicity can be understood in terms of evolutionary timescales of binary systems. The detection of Li in SDSS J1035+0641 places a strong constraint on theories that aim at solving the cosmological lithium problem. The Li abundance of the two warmer stars at $[\text{Fe}/\text{H}] \sim -4.0$ places them on the Spite plateau, while the third, cooler star, lies below.

We argue that this suggests that the temperature at which Li depletion begins increases with decreasing $[\text{Fe}/\text{H}]$. SDSS J1349+1407 may belong to a class of Mg-rich EMP stars. We cannot assess if there is a scatter in α -to-iron ratios among the EMP stars or if there are several discrete populations. However, the existence of stars with low α -to-iron ratios is supported by our observations.

Key words. Stars: Population II - Stars: abundances - Galaxy: abundances - Galaxy: formation - Galaxy: halo

1. Introduction

Extremely metal-poor (EMP) stars are the shining witnesses of a primordial Universe corresponding to a redshift higher than 10. They belong to the second generation of stars, objects formed from the gas enriched only by the first generation of the stars, Pop III stars. Direct observation at high redshift of the individual massive Pop III stars is not feasible because they are too

faint for the current and next generation of telescopes. There is one possible exception. In the case of Pop III stars formed with masses of a few hundred M_{\odot} (Hirano et al. 2014), they could have ended their life with a pair-instability supernovae (PISN) event. According to Bromm (2014), this kind of event could be visible for the James Webb Space Telescope (JWST) planned to be launched in 2019. However, even in this event it is unlikely that the low-resolution spectra that could be obtained from JWST would be able to provide a detailed chemical inventory of PISN ejecta. At the moment, EMP stars are the only way to deduce the characteristics of the Universe at the time they formed.

Send offprint requests to: P. Bonifacio

[★] Based on observations obtained at ESO Paranal Observatory, Programmes 189.D-0165,090.D-0306, 093.D-0136, 096.D-0468

Table 1. SDSS DR12¹ photometry and exposure times for the programme stars.

Star	<i>u</i>	<i>g</i>	<i>r</i>	<i>i</i>	<i>z</i>	T_{exp} s	N_{exp}
SDSS J014036.22+234458.0	16.78	15.82	15.35	15.12	15.03	3005	1
SDSS J103402.71+070116.6	18.34	17.52	17.23	17.13	17.12	3005	5
SDSS J103556.11+064143.9	19.53	18.65	18.37	18.31	18.26	3005	29
SDSS J124719.46-034152.4	19.32	18.50	18.24	18.15	18.14	3005	5
SDSS J134922.91+140736.9	17.44	16.65	16.33	16.24	16.19	3600	9
SDSS J144256.37-001542.8	18.76	17.96	17.65	17.51	17.49	3005	3
SDSS J150702.02+005152.6	19.75	18.77	18.57	18.48	18.41	3005	6

¹In this work we used the SDSS DR12 photometry; the magnitudes of the latest release DR14, differ from these values by less than 0.015 mag.

The TOPoS project (Caffau et al. 2013b) has been designed to increase the number and chemical inventory of EMP turn-off stars. The TOPoS targets were selected from the stars observed spectroscopically in the SDSS/SEGUE/BOSS survey with the following colour cuts: $0.18 \leq (g - z)_0 \leq 0.70$ and $(u - g)_0 > 0.70$. This allows the identification of stars likely to be close to the main sequence turn-off of halo stars.

2. Observations and data reduction

Target stars were observed using the ESO Ultraviolet and Visual Echelle Spectrograph (UVES, Dekker et al. 2000) mounted at the Kueyen 8.2m telescope, the second unit telescope of the Very Large Telescope (VLT, Cerro Paranal, Chile). Observations of five stars were collected in service mode in the course of Large Programme 189.D-0165 (PI E. Caffau) between April 2013 and March 2016. We adopted setting Dic 1 390+580 and therefore observed simultaneously with the blue and red UVES arms, centred at 390 nm and 580 nm, and covering the spectral ranges 326-454 nm and 476-684 nm, respectively. The data were binned 2×2 (spectral \times spatial direction), and a $1.4''$ slit width was adopted. This resulted in a resolving power of $R \approx 30000$ or larger when the image quality was better than $1.4''$. A different number of 3005 s frames were taken for six of the target stars, namely 1, 5, 11, 5, 3, and 6 for stars SDSS J0140+2344, SDSS J1034+0701, SDSS J1035+0641, SDSS J1247-0341, SDSS J1442-0015, and SDSS J1507+0051, respectively. The signal-to-noise ratios per pixel of individual spectra varied in the range 3-30 for the blue arm and 8-61 for the red arm.

Star SDSS J1035+0641 was also observed with setting Dic 2 437+760 (programme ID: 096.D-0468 PI Sbordone), with the blue and red arms covering the spectral ranges 373-499 nm and 565-946 nm, respectively. A total of 18×3005 sec frames were acquired. The same slit width ($1.4''$) and on-chip binning (2×2) were chosen. Signal-to-noise ratios per pixel of individual spectra varied in the range 5-10 and 4-8 for the blue and red arms, respectively.

SDSS J1349+1407 was observed in service mode in the course of programmes 090.D-0306 and 093.D-0136 (PI Sbordone) between March 2013 and June 2014. The setting used in this case was Dic2 437+760 with a 1×1 binning and a $1.0''$ slit, providing a resolving power of $R \sim 48000$. A total of nine integrations of 3600s each were acquired. The coadded spectrum attains a S/N ~ 40 per pixel at 400 nm and a S/N ~ 60 per pixel at 590 nm.

The data were reduced by the ESO staff, and retrieved through the Phase 3 spectral data products query form¹.

3. Analysis

The chemical analysis has been done with the code MyGIsFOS (Sbordone et al. 2013). This code derives the chemical abundances by fitting a selected set of features. The best fit profile is obtained by interpolating in a series of pre-calculated synthetic spectra. These synthetic spectra have been computed with turbospectrum (Alvarez & Plez 1998; Plez 2012) and are based on a grid of 1D plane-parallel hydrostatic model atmospheres previously computed with MARCS (Gustafsson et al. 2008). The procedure to derive the atmospheric parameters and chemical composition is described by Caffau et al. (2013b) and has also been used in the other papers of this series (Bonifacio et al. 2015; Caffau et al. 2016). There were two exceptions for which MyGIsFOS was not well adapted: carbon in all stars, and magnesium in the star SDSS J1349+1407. Carbon was derived by χ -squared fitting of the G-band with a specifically computed grid of synthetic spectra with fixed metallicity, T_{eff} , and $\log g$ and with varying C abundance. This technique is the same as that used in our previous papers (Spite et al. 2013; Bonifacio et al. 2015). To take into account the known granulation effects on the G-band (Collet et al. 2007; Behara et al. 2010; Gallagher et al. 2016, 2017), we used the corrections provided by Gallagher et al. (2016), assuming a metallicity of -3.0 . The stellar parameters and abundances of C and Li are provided in Table 2.

Because its [Mg/Fe] ratio is so extreme (Mg enhanced by more than 1 dex over Fe), one concern for SDSS J1349+1407 was that its temperature structure could be different from that of a normal solar-scaled and α -enhanced model. Magnesium is one of the main electron donors for solar-type stars, and its abundance may affect the ionisation structure of the atmosphere. We verified that the high [Mg/H] does not affect the abundances derived with models enhanced in Mg by the canonical 0.4 dex by computing both the ATLAS 9 and ATLAS 12 models (Kurucz 1993, 2005; Sbordone et al. 2004; Sbordone 2005), the latter with [Mg/Fe]=+1.4 to derive the abundances. From this test we conclude that the differences are negligible; the largest difference reaches 0.05 dex for Mn. At the very low metallicities relevant for the stars analysed in this paper, Mg, Ca, and any metals cease to be important electron donors; as already discussed by Christlieb et al. (2004), the main electron donor is, in fact, hydrogen.

3.1. Individual stars and comparison with previous analyses

All of our targets have already been analysed by our group on the basis of X-Shooter spectra, and some have also been analysed by other groups.

- SDSS J0140+2344. The stellar parameters and [Fe/H] we derive are in excellent agreement with those determined by Caffau et al. (2013b) from the analysis of an X-Shooter spectrum. Our estimated upper limit of A(C) from the X-Shooter spectrum was too optimistic: the carbon abundance we derive in this work is 0.3 dex larger than the X-Shooter upper limit.

The Mg and Si abundances measured from the X-Shooter and UVES spectra are in excellent agreement.

¹ http://archive.eso.org/wdb/wdb/adp/phase3_spectral/form

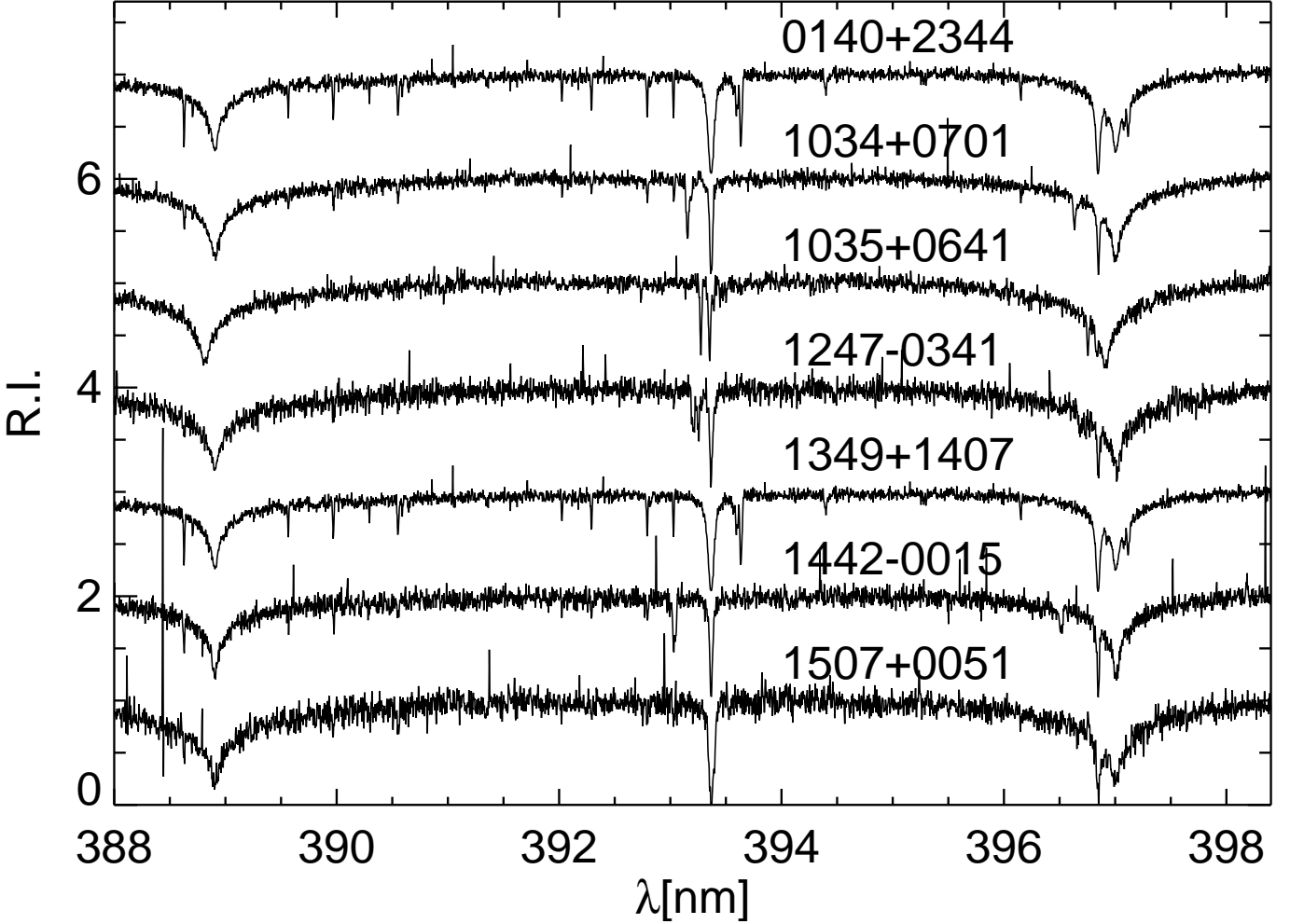


Fig. 1. Spectral ranges of the Ca II-H and -K lines of the sample stars.

The Ca abundance measurements are more problematic. We detect two Ca I lines, the resonance line at 422.67 nm and the subordinate line at 442.54 nm. The two lines are very discrepant, as is generally the case in EMP stars, even when NLTE effects are taken into account (see Spite et al. 2012, and references therein). The 422.67 nm resonance line provides $[Ca/H] = -3.97$, in good agreement with the X-Shooter spectrum where the only Ca I line detected was in fact the 422.67 nm line, which implied $[Ca/H] = -3.78$. The subordinate line yields a Ca abundance that is over 1 dex higher ($[Ca/H] = -2.79$). In Table 3 we only provide the value from the subordinate line, which, as discussed by Spite et al. (2012), is more reliable. The Ca II is derived from the K-line alone and it is a factor of three lower than the value we had estimated from the X-Shooter spectrum; however, in that case we relied only on the Ca II infrared triplet lines. The abundance from the K-line is also strongly discrepant from the Ca I subordinate line. Yong et al. (2013) analysed a Keck/HIRES spectrum of this star. They derived $T_{\text{eff}} = 5703$ K from a combination of spectrophotometry and Balmer line analysis. This is in agreement, within the errors, with our adopted T_{eff} . The surface gravity was derived from isochrones and two solutions were found, depending on whether the star is a main sequence or a subgiant star, this corresponds to $\log g = 3.36$

or $\log g = 4.68$. In the two cases, they derive $[Fe/H] = -4.11$ or $[Fe/H] = -4.02$ (with our adopted solar Fe abundance Caffau et al. 2011a), in excellent agreement with our result. For Ca, they only measure the Ca I 422.67 nm resonance line and derive $[Ca/H] = -3.82$ or $[Ca/H] = -3.88$, again in excellent agreement with our results for the same line.

Aoki et al. (2013) analysed a Subaru spectrum of this star and used $T_{\text{eff}} = 6103$ K, which was derived from the SDSS low-resolution spectrum by the SEGUE Stellar Parameter Pipeline (SSPP, Lee et al. 2008), even though both $V - K$ and $g - r$ imply a temperature close to that used by us. For the surface gravity they assumed $\log g = 4.0$ and, like us, they derived $[Fe/H] = -3.67$ (on our adopted solar abundance scale). Considering their adopted higher effective temperature, this metallicity is consistent both with ours and with that of Yong et al. (2013). For Ca they derive $[Ca/H] = -3.82$ from a single line. Although it is not explicitly stated, it is highly probable that this refers to the Ca I 422.67 nm resonance line.

Finally, Aguado et al. (2016) analysed the SDSS spectrum and a ISIS WHT spectrum and derived the stellar parameters 6090 ± 200 K/ 4.7 ± 0.3 / -3.6 ± 0.2 . Unsurprisingly, the T_{eff} is close to the SSPP value and the derived metallicity is consistent.

We conclude that the different analyses of this star are all consistent, but we point out the discrepancy of the Ca abun-

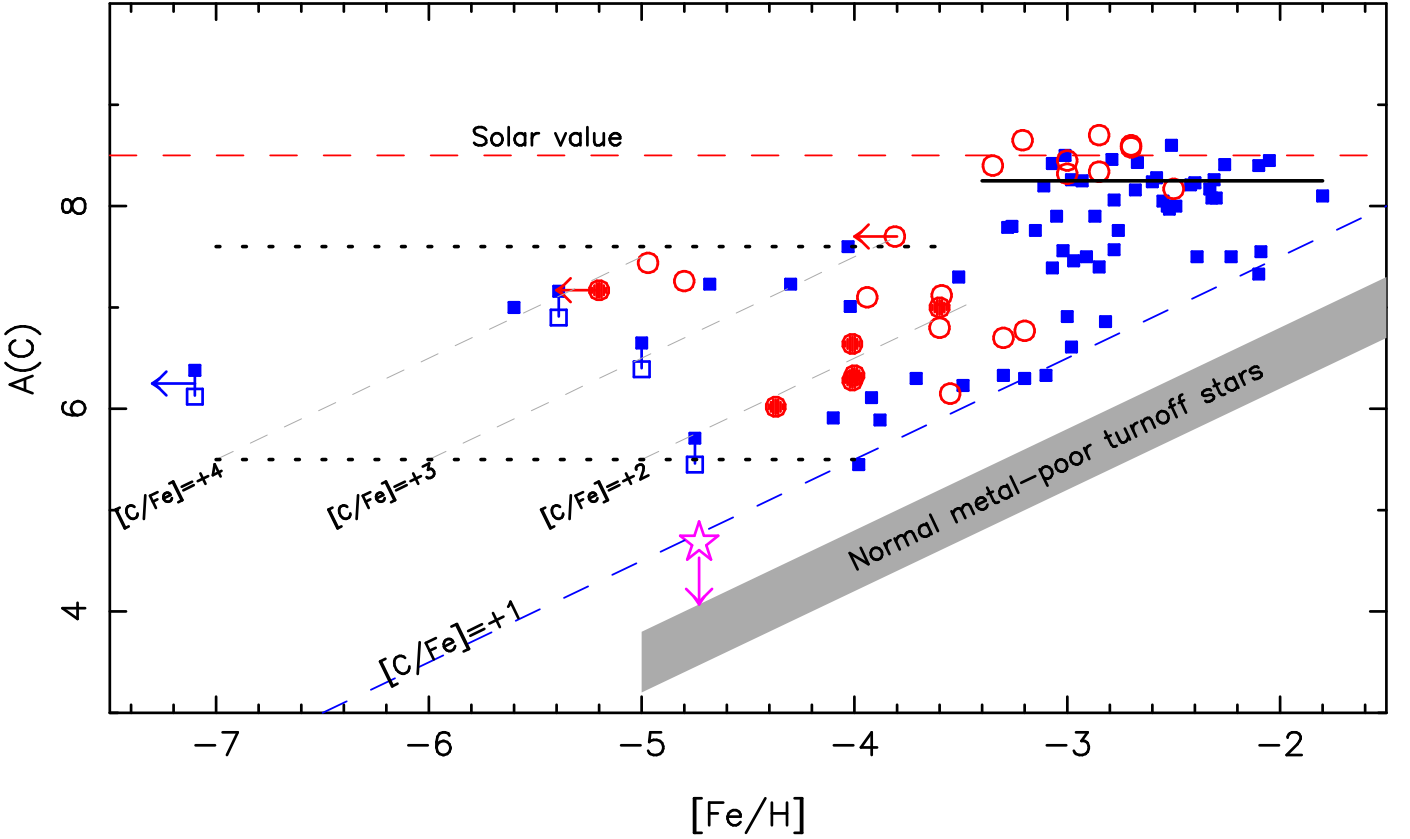


Fig. 2. Carbon abundances of the programme stars (filled red circles)

as a function of $[\text{Fe}/\text{H}]$. Other stars published by our group are shown as open red circles. Other stars from the literature (Sivarani et al. 2006; Plez & Cohen 2005; Plez et al. 2005; Frebel et al. 2005, 2006; Thompson et al. 2008; Aoki et al. 2008; Behara et al. 2010; Masseron et al. 2010, 2012; Yong et al. 2013; Cohen et al. 2013; Li et al. 2015b) are shown as blue squares. The violet star is the upper limit on SDSS J1029+1729 (Caffau et al. 2011b, 2012). The horizontal dotted lines delimit the low-carbon band.

dance derived from different lines. This will have to be revisited in the light of 3D NLTE computations in the future.

- SDSS J1034+0701. The X-Shooter spectrum is analysed in François et al. (2017). The $[\text{Fe}/\text{H}]$ from the UVES spectrum is about 0.4 dex lower than the value derived from the X-Shooter spectrum. The Mg abundance is in agreement within errors. We did not derive the Ca abundance from the UVES spectrum, but the Ca abundance from the X-Shooter spectrum, based on the Ca II IR triplet, and the X-Shooter based Fe abundance implies $[\text{Ca}/\text{Fe}] = +0.33$.
- SDSS J1035+0641. Bonifacio et al. (2015) investigated an X-Shooter spectrum, but they could only derive $A(\text{C})$ and an upper limit for the Fe abundance. The $A(\text{C})$ derived from the UVES spectrum is a factor of two higher than the value we derived from the X-Shooter spectrum, which illustrates the limit of measuring the G-band for a warm star like this at moderate resolution. The non-detection of the 382.0425 nm line (equivalent width < 0.4 pm at 1σ) provides an upper limit of the Fe abundance $[\text{Fe}/\text{H}] < -5.2$, tighter than the value we derived from the X-Shooter spectrum. A fit to the Ca II K line provides an abundance that is consistent with that derived from the X-Shooter spectrum.

We found a mistake in Table 7 of Bonifacio et al. (2015) and in their Figure 10. The upper limit on lithium, corresponding to an upper limit of 1.8 pm, is $A(\text{Li}) < 2.05$ and not 1.1, as incorrectly listed in Table 7. Our measured equivalent width

of 1.3 pm is consistent with that upper limit and corresponds to $A(\text{Li}) = 1.90$.

- SDSS J1247–0341. The metallicity determined by Caffau et al. (2013b) from the X-Shooter spectrum is in good agreement with that derived from the UVES spectrum. Also in this case the C abundance derived from the UVES spectrum is larger by 0.6 dex than the value we estimated from the X-Shooter spectrum. The Mg abundances from X-Shooter and UVES spectra are consistent within 1σ . Caffau et al. (2013b) provided the Ca abundance from two lines of the Ca II IR triplet, which we considered more reliable than the Ca I 422.67 nm resonance line. That line implied $[\text{Ca}/\text{H}] = -3.96$, which is consistent with the abundance provided here for the same line. Also in this case we point out how different lines provide different abundances for Ca; this is likely due to the inadequacy of the 1D LTE analysis of this element in these extremely metal-poor stars. The Gaia data release 1 (Gaia Collaboration et al. 2016) shows that this star has a close-by companion at a distance of $0''.01$ and 0.5 mag fainter in G . Certainly the light of this companion contaminates our spectrum, but since we do not have any colour information at this time we did not attempt to correct our spectrum for the veiling. We do not detect any sign of the spectrum of the companion star in our spectrum.
- SDSS J1349+1407. Sbordone et al. (2012) announced it as a Mg-rich star. The quality of the spectrum available at that

time was sufficient only for giving abundances of a few elements. The star was independently recovered as a Mg-rich star by Li et al. (2014), who analysed the SDSS DR9 spectra. Their temperature for the star is higher by 230 K and consequently their metallicity is higher ($[\text{Fe}/\text{H}] = -2.83$). In the UVES spectrum of SDSS J1349+1407 we identified six Mg I lines in the blue spectrum (382.9, 383.2, 383.8, 405.7, 416.7, 470.2 nm). We fitted the line profiles and we derived $A(\text{Mg}) = 5.30 \pm 0.16$ and by removing the line which is in the wing of a Balmer line, we derive $A(\text{Mg}) = 5.36 \pm 0.11$. The star is also enhanced in Na, with $[\text{Na}/\text{Fe}] = +0.86$.

- SDSS J1442–0015. We compared our spectrum with the X-Shooter spectrum of Caffau et al. (2013a). The metallicities from the analysis of the two spectra are in good agreement within errors of less than 1σ . The Mg abundances are in reasonable agreement with 1.5σ errors. The situation is slightly worse for the Ca abundance; the abundances derived from the Ca I 422.67 nm resonance line from the two spectra are consistent to within 1.8σ , i.e. 0.7 dex. As usual, this is discrepant with the Ca II IR triplet lines, measured in the X-Shooter spectrum. This example is a recommendation not to overinterpret the abundances that rely on a single, weak line. It is important to note that both here and in the study of Caffau et al. (2013a)

we adopted the effective temperature derived by fitting the wings of $H\alpha$, which is considerably lower than the temperature implied by the $g - z$ colour (6161 K).

- SDSS J1507+0051. The X-Shooter spectrum was analysed by Caffau et al. (2013b). Both the metallicity and the Mg abundance of the two analyses are in agreement within less than 1σ . Instead, we have a strong discrepancy for the abundances of Ca derived from Ca II lines. In the UVES spectrum we detect the 370.6024 nm line, while in the X-Shooter spectrum, we relied on the IR triplet lines. This discrepancy needs to be further investigated.

4. Results and discussion

The main result of this investigation is the confirmation, based on higher resolution spectra, of the very low metallicities that we derived for these stars from the analysis of the X-Shooter spectra. Two stars have $[\text{Fe}/\text{H}]$ below -4.3 , three stars around -4.0 , and two stars around -3.5 . These numbers confirm the high efficiency of the TOPoS strategy for target selection. The five stars with $[\text{Fe}/\text{H}] \leq -4.0$ discussed in this paper, SDSS J1742+2531 ($[\text{Fe}/\text{H}] = -4.80$, Bonifacio et al. 2015) and SDSS J0929+0238 ($[\text{Fe}/\text{H}] = -4.97$, Caffau et al. 2016) are the most iron-poor stars we found in the course of the TOPoS project and they are all strongly C-enhanced. To date, among the stars with $[\text{Fe}/\text{H}] \leq -4.5$ the only ‘non C-enhanced star’ found is SDSS J1029+1729 (Caffau et al. 2011b, 2012).

4.1. Carbon abundances

It is interesting to note that all the C-enhanced stars that we have found belong indeed to the low-carbon band discussed by Bonifacio et al. (2015), as illustrated in Fig. 2. These stars do not seem to be enhanced in s -process elements and we suggest that they are indeed CEMP-no stars. This view is supported also by the recent study of Hansen et al. (2016) who analysed a sample of 27 metal-poor stars and found that 20 of them are CEMP, 3 of which are CEMP-no stars that belong to the low-carbon band.

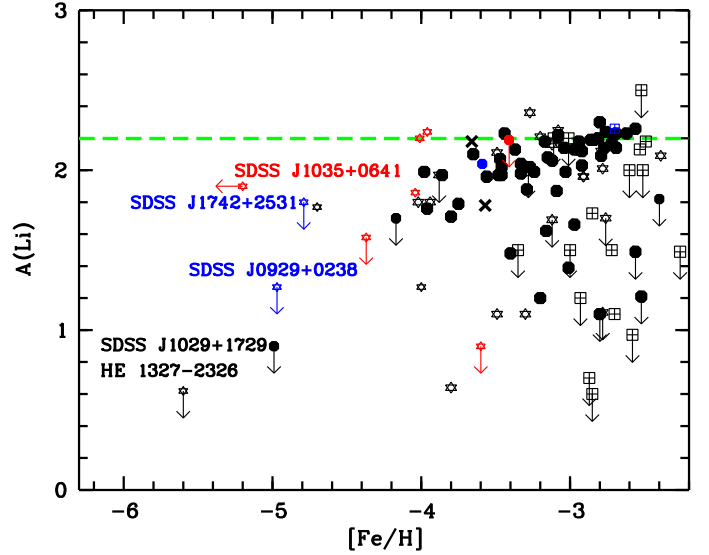


Fig. 3. Lithium abundance in unevolved extremely metal-poor stars. The different symbols refer to different carbon abundances. The filled hexagons refer to carbon normal stars. CEMP stars of the low- and high-carbon bands are shown as star symbols and crossed squares, respectively. Measurements and upper limits of the programme stars are shown in red. Measurements and upper limits from our group’s previous papers (Bonifacio et al. 2015; Caffau et al. 2016) are shown in blue. Black symbols are stars for which metallicity, lithium abundance, and carbon abundance are taken from the literature (Norris et al. 1997; Lucatello et al. 2003; Sivarani et al. 2004; Ivans et al. 2005; Sivarani et al. 2006; Frebel et al. 2007, 2008; Thompson et al. 2008; Aoki et al. 2008; Sbordone et al. 2010; Behara et al. 2010; Caffau et al. 2012; Carollo et al. 2012; Masseron et al. 2012; Aoki et al. 2013; Ito et al. 2013; Carollo et al. 2013; Spite et al. 2013; Roederer et al. 2014; Aoki 2015; Bonifacio et al. 2012; Li et al. 2015b; Hansen et al. 2014; Caffau et al. 2016; Placco et al. 2016; Matsuno et al. 2017). The two components of the binary system CS 22876-32 (González Hernández et al. 2008) are shown as black crosses. The green dashed line is the level of the Spite plateau as determined by Sbordone et al. (2010).

We suggest here that a useful classification of metal-poor stars can be made using only their C abundance without any reference to their abundance of n -capture elements. This is related to the fact that, for unevolved stars, it is very difficult to secure data quality high enough to derive measurements or significant upper limits for the heavy elements. Our proposed classification scheme is as follows:

- ‘carbon normal’: for $[\text{Fe}/\text{H}] \geq -4$ $[\text{C}/\text{Fe}] < 1.0$, for $[\text{Fe}/\text{H}] < -4$ $A(\text{C}) < 5.5$;
- low-carbon band CEMP stars: stars that do not fulfil the carbon normal criterion and have $A(\text{C}) \leq 7.6$;
- high-carbon band CEMP stars: stars that do not fulfil the carbon normal criterion and have $A(\text{C}) > 7.6$.

This classification is qualitatively similar to that proposed by Yoon et al. (2016), except that their Group II is partly included in our low-carbon band and mostly in our carbon normal stars, their Group I is by and large coincident to our high-carbon band, except for the stars with the lowest C abundances in their Group I, which we assign to the low-carbon band.

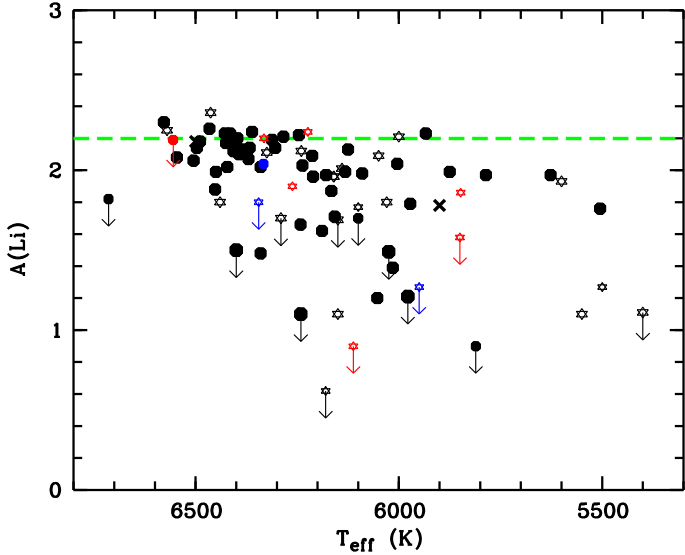


Fig. 4. Lithium abundance in the unevolved extremely metal-poor stars as a function of effective temperature. The meaning of the symbols is the same as in Fig. 3. The high-carbon band CEMP stars have not been included in this plot.

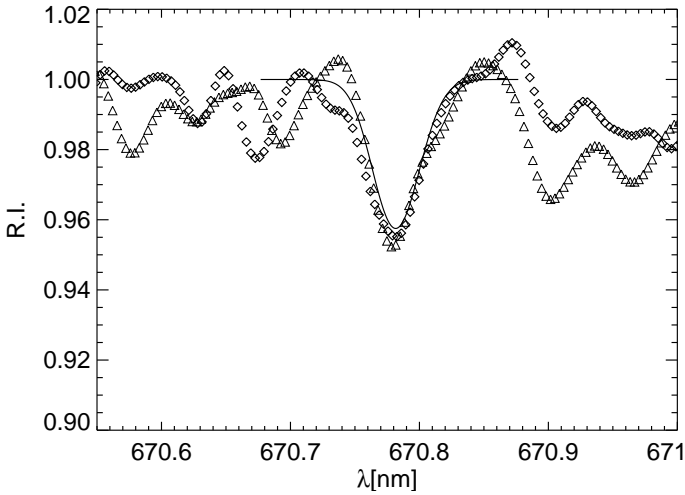


Fig. 5. Lithium doublet in SDSS J1034+0701 (squares) and SDSS J1247-0341 (triangles) compared to a 3D NLTE theoretical profile ($T_{\text{eff}} = 6270 \text{ K}$, $\log g = 4.0$, $[M/H] = -3.0$, $A(\text{Li}) = 2.1$). The observed spectra have been smoothed with a Gaussian of 4 km s^{-1} FWHM to increase the S/N.

In Bonifacio et al. (2015) we also used the working hypothesis that all the stars on the high-carbon band are binaries and the high carbon abundance is the consequence of mass-transfer from a companion during its AGB phase. This hypothesis, however, does not place any lower limit to the $[\text{Fe}/\text{H}]$ of the high-carbon band stars. The fact that, observationally, we do not find any high-carbon band stars below $[\text{Fe}/\text{H}] = -3.6$ is intriguing. In Fig. 2 we have 26 stars with a metallicity below -3.6 , of which 25 are C-enhanced, and none is a high-carbon band star. It therefore seems unlikely to admit that this is just the result of small number statistics. The binary systems that can give rise to a high-carbon band star, in our hypothesis, are severely constrained regarding the masses of the components.

In particular, the primary star should be larger than about $0.9M_{\odot}$ to experience efficient third-dredge-up episodes during the AGB phase (Stancliffe & Glebbeek 2008; Karakas 2010), and consequently enrich its surface with the carbon produced in the stellar interior. The secondary should be less massive than about $0.8 - 0.85M_{\odot}$, because higher-mass stars would become white dwarfs on a timescale shorter than $10 - 12$ billion years, which is the approximate age of the Galactic halo. Finally, mass transfer in binary systems with AGB donors is efficient in a limited range of orbital periods between approximately 10^2 and 10^5 days (e.g. Izzard et al. 2009; Abate et al. 2015).

Campbell & Lattanzio (2008) computed the yields of AGB stars of extremely low and zero metallicity, and they found that the $[\text{C}/\text{Fe}]$ ratios of their yields increase monotonically with decreasing $[\text{Fe}/\text{H}]$ (as illustrated in their Figure 5). The carbon abundance in the ejecta of the AGB star varies within a factor of four in the metallicity range $-6.5 \leq [\text{Fe}/\text{H}] \leq -3.0$ (Campbell & Lattanzio 2008). Therefore, theoretically, there is no indication that the nucleosynthetic yields of AGB stars vary in metallicity in such a way as to disfavour the formation of high-carbon band stars.

A possible explanation of the lack of high-carbon band stars at low $[\text{Fe}/\text{H}]$ is that at these metallicities, such systems either do not form at all or are exceedingly rare. The existence of a rather sharp cut-off suggests the existence of a physical mechanism that prevents the formation of these systems. Because the enriched material synthesised by the AGB star needs to be expelled in the stellar wind and accreted by a low-mass companion, the lack of high-carbon band stars could indicate that at low $[\text{Fe}/\text{H}]$ binary mass-transfer processes become rarer or less efficient. Although the binary-star fraction is not well constrained at low metallicity, there is no evidence that it decreases (e.g. Gao et al. 2014). The data on the binarity among stars with $[\text{Fe}/\text{H}] < -3.6$ is scanty, yet the discovery of the binarity of SDSS J0929+0238 (Caffau et al. 2016) suggests that it cannot be much lower than among stars of higher metallicity. It has been suggested that at low metallicity the ejection of the AGB envelope becomes increasingly inefficient (Wood 2011). If only a small mass is ejected by the primary, the amount of material accreted by the secondary may be insufficient to enhance the carbon abundance up to a typical high-carbon band value.

Another effect to take into account is that when a star accretes material and becomes more massive, it evolves more quickly than a single star of equal initial mass. In the simulations of Abate et al. (2015) the synthetic population of CEMP-*s* stars has typically accreted a mass of approximately $0.1M_{\odot}$. Stars with initial mass $0.8M_{\odot}$ at low metallicity have a lifetime of approximately the age of the Universe; however, if they experienced binary mass-transfer they would become high-carbon band CEMP-*s* stars of mass $\approx 0.9M_{\odot}$ and consequently their lifetimes would be shorter than 12 Gyr. Hence, they would not be visible any longer. Similarly, stars of initial mass of $0.7M_{\odot}$ would reach masses of around $0.8M_{\odot}$ and still be visible after 12 Gyr, but for a shorter time than single stars of the same initial mass. Also, the results of Moe & Di Stefano (2017) suggest that large initial mass ratios $q = M_{2,i}/M_{1,i}$ could be slightly more likely among low-mass binaries, hence increasing the proportion of systems with initial secondary mass $M_{2,i} > 0.8M_{\odot}$. The probability of observing a star at a given distance during its evolution is proportional to the time its apparent luminosity is above our detection threshold. If a star is visible in its main sequence phase, it will also be visible in the RGB phase, but not once it reaches the white dwarf stage, unless it is very near to us. A faster evolu-

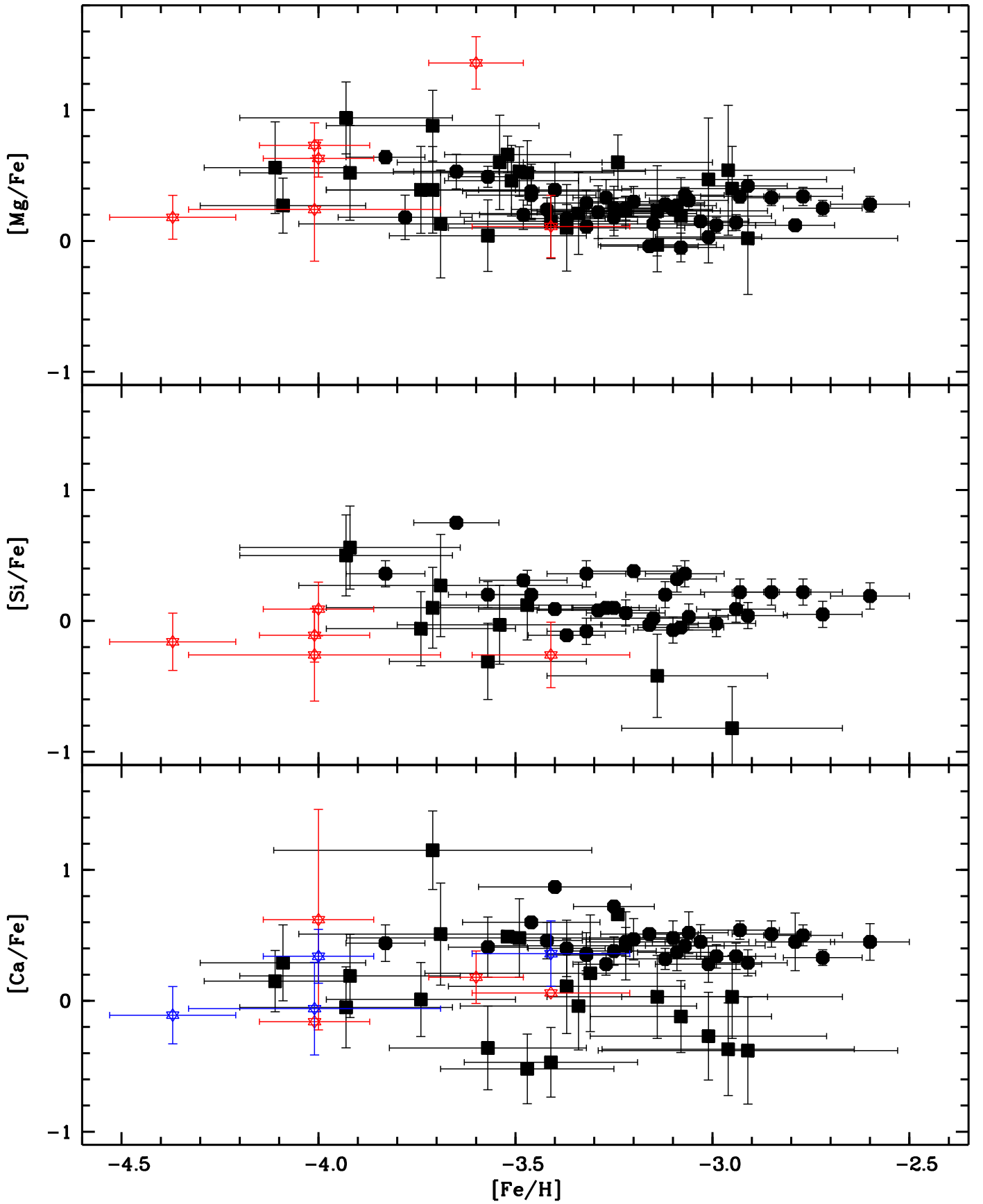


Fig. 6. Ratio of α elements to iron for the programme stars (red stars) compared to those measured by our group in other extremely metal-poor dwarf stars (Bonifacio et al. 2009; Caffau et al. 2011c; Bonifacio et al. 2012; Caffau et al. 2013a,b). Black squares are measurements from X-Shooter spectra, while black hexagons are measurements from UVES spectra. In the panel giving the $[\text{Ca}/\text{Fe}]$ ratio, the blue star symbols are Ca II measures. We restricted the x-axis so as to exclude SDSS J1035+0641; which only has an upper limit on iron and thus a lower limit on $[\text{Ca}/\text{Fe}]$ and is not informative.

ing star reaches the white dwarf stage more quickly and is thus less likely to be observed. The decrease in lifetime of the high-carbon band population, due to their increase in mass, naturally occurs at every metallicity, but its consequences become more evident at $[\text{Fe}/\text{H}] \leq -3.5$ because fewer stars are known in this range.

The determination of the binary fraction and the period distribution for different metallicity bins down to the lowest metallicities may provide a fundamental insight into the properties of star formation at different metallicities.

4.2. Lithium abundances

In Fig. 3 we show the Li abundances as a function of $[\text{Fe}/\text{H}]$ for our programme stars and for stars taken from the literature. We classify the stars in three groups: low-carbon band CEMP stars (star symbols); high-carbon band CEMP stars (crossed squares); and carbon normal stars (filled hexagons), which includes all stars with $[\text{C}/\text{Fe}] < 1.0$ or for which the C abundance has not been measured. From this figure it appears that the Li abundances in the low-carbon band CEMP stars have a behaviour that is indistinguishable from that of the carbon normal stars. On the other hand the high-carbon band CEMP stars are preferentially Li-depleted, although there are a few measurements on the Spite plateau. This is consistent with our hypothesis that the high-carbon CEMP stars are the result of mass transfer from an AGB companion. In most cases Li is depleted as a result of processing in the H-burning AGB shell, although in some cases it may also be produced through the Cameron–Fowler mechanism (Cameron & Fowler 1971). Mass transfer from an AGB companion has been invoked to explain the occurrence of Li-rich main sequence stars in globular clusters (Koch et al. 2011; Monaco et al. 2012), although pollution from nearby RGB stars having undergone the Li-flash is an alternative explanation (Pasquini et al. 2014). The point is that transfer from an AGB always results in an enhancement of carbon, but Li may be either depleted or enhanced.

The stars SDSS J1034+0701 and SDSS J1247–0341 both have $[\text{Fe}/\text{H}] \sim -4.0$. The measurements of the equivalent width of the Li I resonance doublet are very uncertain. In Fig. 5 we show the observed spectra compared to a 3D NLTE synthetic spectrum. We stress that this is not a fit; we just plot the synthetic spectrum to provide guidance to the position and expected strength of the Li I resonance doublet. Although the measurement is uncertain, we believe that the detection of Li is robust. Taken at face value, our measurements place both stars on the Spite plateau. All the other stars have either an upper limit or a measurement that places them well below the Spite plateau. While this behaviour, also referred to as ‘melt-down’ of the Spite plateau (Sbordone et al. 2010, but see also Bonifacio et al. 2007; Aoki et al. 2009), is well known, these two stars on the Spite plateau appear exceptional. In fact, recently Matsuno et al. (2017) pointed out that ‘no star in the literature has comparable Li abundance to the Spite plateau below $[\text{Fe}/\text{H}]$ of -3.5 , except for the primary of the double-lined binary system CS 22876–032.’ The two components of CS 22876–032 are shown as \times symbols in Figs. 3 and 4. While SDSS J1034+0701 and SDSS J1247–0341 have an effective temperature well above 6000 K, as does CS 22876–032 A (González Hernández et al. 2008), the star SDSS J0140+2344 has an effective temperature below 6000 K; it has roughly the same metallicity ($[\text{Fe}/\text{H}] = -4.0$) and, like CS 22876–032 B, it has a Li abundance well below the Spite plateau. Therefore, our observations call into question the claim by Matsuno et al. (2017), that Li abundances in the in-

terval $-4.5 \leq [\text{Fe}/\text{H}] \leq -3.5$ are almost constant at a value lower than the Spite plateau. For stars with $T_{\text{eff}} > 6000$ K, there are some stars on the Spite plateau, at least down to $[\text{Fe}/\text{H}] = -4.0$. On the other hand, among the stars with $T_{\text{eff}} \leq 6000$ K and $[\text{Fe}/\text{H}] \leq -3.5$, lithium is always below the Spite plateau. This can be seen in Fig. 4, where the only star at effective temperature below 6000 K on the Spite plateau is SDSS J0907+0246 ($[\text{Fe}/\text{H}] = -3.44$). The current observations suggest that the T_{eff} for which lithium destruction in the stellar atmospheres becomes important, increases as metallicity decreases, although it is unlikely that this is the only effect that drives Li destruction since there are several stars hotter than 6000 K that are found well below the Spite plateau. Bonifacio & Molaro (1997) argued that for $T_{\text{eff}} \geq 5700$ K Li destruction was negligible; however, their sample had only three stars with metallicity below -3.0 . From Fig. 4 it is clear that with increasing T_{eff} there are fewer stars below the Spite plateau, and, at any rate, the average Li abundance is higher.

Our detection of Li in SDSS J1035+0641 is to date the measurement of Li in the most iron-poor unevolved star. It poses a strong constraint on any theory that aims to explain the cosmological Li problem. Any theory involving stellar destruction of Li must accommodate the fact that in SDSS J1035+0641 Li is measurable.

In other stars of comparable iron abundance, it is either completely destroyed or, at least, more severely depleted. Alternatively, if one tries to explain the Li abundance of this star by a prompt enrichment in Li, one has to explain why such a prompt enrichment has not taken place in the other stars with $[\text{Fe}/\text{H}] \leq -5.0$.

4.3. Abundances of other elements

One of the main goals of the UVES observations was to increase the chemical inventory of the stars at very low metallicity. The data presented in Table 3 fulfil this goal, although the low metallicities of the stars imply that we have many upper limits. We have two measurements of Co that confirm that Co is enhanced over Fe in EMP stars, as already shown by Cayrel et al. (2004) and Bonifacio et al. (2009). In the two cases where Sr is measured, it is enhanced over Fe; however, this is certainly a selection effect since for a given effective temperature, the higher the abundance, the stronger the line and thus the easier it is to detect it.

In Fig. 6 we provide the ratios of the measured α elements, Mg, Si, and Ca, to Fe. In the upper panel, SDSS J1349+1407 clearly stands out as being extremely enhanced in Mg, although its Ca abundance seems quite normal. There is another star in our sample, SDSS J1050+2421 (Caffau et al. 2013b), that is highly enhanced in Mg, although not as much as SDSS J1349+1407. We note that there is a discrepancy of about 1 dex in the Ca abundance of SDSS J1050+2421 derived from the Ca I resonance line or from the Ca II lines. This discrepancy may be partly due to an incorrect gravity, since a discrepancy of about 0.5 dex is found between the iron abundances derived from the Fe I and Fe II lines (Caffau et al. 2013b). Based on its proper motion, it has been pointed out that this star is most probably a main sequence star with a $\log g \sim 4.7$, rather than 4.0, as was assumed in Caffau et al. (2013b) (M. Bessell, private communication). The $[\text{Ca I}/\text{Fe I}]$ and the $[\text{Ca II}/\text{Fe II}]$ ratios differ by ‘only’ about 0.6 dex.

Thus, a change in gravity may alleviate the problem, but not solve it. In Fig. 6 we plot the value derived from the Ca I resonance line. Had we chosen the value derived from Ca II, SDSS J1050+2421 would be highly enhanced in Ca as well.

The abundances of SDSS J1349+1407 resemble very closely those of CS 22949-037 (Depagne et al. 2002; Norris et al. 2002); in fact, they have almost the same $[Mg/Ca]$ (~ 1.2). Among the EMP stars, a $[Mg/Ca]$ almost as high is found for HE 1327-2326 (Frebel et al. 2008 $[Mg/Ca]=0.99$) and an even higher value is found in SMSS J0313-6708 (Keller et al. 2014) $[Mg/Ca]=2.95$. Both CS 22949-037 and HE 1327-2326 are enhanced in Na: $[Na/Fe]=+1.57$ (Andrievsky et al. 2007) and $[Na/Fe]=+0.94$ (Frebel et al. 2008). Star HE 1012-1540, analysed at high resolution by the OZ project (Cohen et al. 2013), also seems to belong to this group ($[Mg/Ca]=+0.83$, $[Na/Fe]=+1.02$). Quite intriguingly, a star with similar properties has been found in the Hercules ultra faint dwarf galaxy (Koch et al. 2008). For Her-2, with $[Mg/Ca]=+0.93$ and $[Na/Fe]=+0.78$, Koch et al. (2008) argued that this may be understood in terms of enrichment from very massive stars with masses of the order of $30 M_{\odot}$.

The other feature that stands out in Fig.6 is that we find additional stars with low α -to-iron ratios, for example SDSS J1442-0015 and SDSS J1247-0341. This confirms our earlier claim (Caffau et al. 2013a), based on X-Shooter spectra, regarding the existence of a population of extremely metal-poor α -poor stars. The presence of metal-poor stars with low α -to-iron ratios, in some cases quite extreme (Ivans et al. 2003), is also supported by other investigations (Cohen et al. 2013; Susmitha Rani et al. 2016). Recently Hayes et al. (2017) also recognised the presence of an α -poor population of stars belonging to the Galactic Halo, albeit at a higher metallicity regime than the one considered in this paper. The presence of these α -poor stars has so-far received little theoretical attention. While Ivans et al. (2003) has invoked a prompt enrichment by type Ia supernovae, Cohen et al. (2013) has suggested that the diversity in nucleosynthesis products of extremely metal-poor type II supernovae is greater than that predicted by current models. These stars could have formed in low-mass dwarf galaxies and subsequently accreted to the Milky Way Halo, carrying memory of a different chemical evolution, as has been claimed by Hayes et al. (2017).

5. Conclusions

We have provided detailed abundances for a sample of seven EMP turn-off stars, based on high-resolution spectra. All the stars for which carbon could be measured are CEMP stars and belong to the low-carbon band. For the most iron-poor star, SDSS J1035+0641, we are unable to detect any iron lines, but we were able to place a stringent upper limit at $[Fe/H] \leq -5.2$. It is remarkable that we measure Li in this star, albeit well below the Spite plateau. This is the first measurement of Li in an unevolved star with $[Fe/H] \leq -5$, and it places a strong constraint on any theory to explain the cosmological Li problem. Three of the programme stars have $[Fe/H] \sim -4.0$, and lithium has been measured in all three. Quite interestingly, the Li abundance of the two warmer stars places them squarely on the Spite plateau, while the cooler one lingers below. This situation is reminiscent of what is observed in the binary system CS 22876-32 (González Hernández et al. 2008). We have argued that this suggests that the effective temperature at which Li depletion begins increases with decreasing $[Fe/H]$.

We confirmed that SDSS J1349+1407 is extremely enhanced in Mg but not in Ca, and in fact its abundance pattern resembles that of CS 22949-037 and its Mg/Ca is also similar to that of HE 1327-2326. This may suggest that there is a class of Mg-rich stars among EMP stars.

Our high-resolution observations have confirmed the existence of stars with low α -to-iron ratios, as pointed out by Caffau

et al. (2013a), based on medium-resolution X-Shooter spectra. The TOPoS project has been very successful in increasing the number of stars with detailed abundances at and below a $[Fe/H]$ of -4.0 , yet the numbers are still smaller than desirable for making robust statistical inferences. Hopefully the Pristine survey (Starkenburger et al. 2017; Caffau et al. 2017; Youakim et al. 2017) and its massive follow-up with WEAVE (Dalton et al. 2016) will soon boost the numbers, and the LAMOST survey as well (Li et al. 2015a,b).

Acknowledgements. We are grateful to our referee Mike Bessell for his very thorough and useful report of our paper. The project is supported by fondation MERAC. N.C., H.G.L., and A.J.G. were supported by Sonderforschungsbereich SFB 881 “The Milky Way System” (subproject A4) of the German Research Foundation (DFG). R.S.K. acknowledges support from the European Research Council via the Advanced Grant “STARLIGHT: Formation of the First Stars” (project number 339177). C.A. acknowledges funding from the Alexander von Humboldt Foundation

References

- Abate, C., Pols, O. R., Stancliffe, R. J., et al. 2015, *A&A*, 581, A62
 Aguado, D. S., Allende Prieto, C., González Hernández, J. I., et al. 2016, *A&A*, 593, A10
 Alvarez R., Plez B., 1998, *A&A* 330, 1109
 Andrievsky, S. M., Spite, M., Korotin, S. A., et al. 2007, *A&A*, 464, 1081
 Aoki, W., Beers, T. C., Sivarani, T., et al. 2008, *ApJ*, 678, 1351
 Aoki, W., Barklem, P. S., Beers, T. C., et al. 2009, *ApJ*, 698, 1803
 Aoki, W., Beers, T. C., Lee, Y. S., et al. 2013, *AJ*, 145, 13
 Aoki, W. 2015, *ApJ*, 811, 64
 Behara, N. T., Bonifacio, P., Ludwig, H.-G., Sbordone, L., González Hernández, J. I., & Caffau, E. 2010, *A&A*, 513, A72
 Bonifacio, P., & Molaro, P. 1997, *MNRAS*, 285, 847
 Bonifacio, P., Molaro, P., Sivarani, T., et al. 2007, *A&A*, 462, 851
 Bonifacio, P., et al. 2009, *A&A*, 501, 519
 Bonifacio, P., Sbordone, L., Caffau, E., et al. 2012, *A&A*, 542, A87
 Bonifacio, P., Caffau, E., Spite, M., et al. 2015, *A&A*, 579, A28
 Bromm, V. 2014, *Science*, 345, 868
 Caffau, E., Ludwig, H.-G., Steffen, M., Freytag, B., & Bonifacio, P. 2011a, *Sol. Phys.*, 268, 255
 Caffau, E., Bonifacio, P., François, P., et al. 2011b, *Nature*, 477, 67
 Caffau, E., Bonifacio, P., François, P., et al. 2011c, *A&A*, 534, A4
 Caffau, E., Bonifacio, P., François, P., et al. 2012, *A&A*, 542, A51
 Caffau, E., Bonifacio, P., François, P., et al. 2013a, *A&A*, 560, A15
 Caffau, E., Bonifacio, P., Sbordone, L., et al. 2013b, *A&A*, 560, A71
 Caffau, E., Bonifacio, P., Spite, M., et al. 2016, *A&A*, 595, L6
 Caffau, E., Bonifacio, P., Starkenburg, E., et al. 2017, *AN*, 338, 686
 Cameron, A. G. W., & Fowler, W. A. 1971, *ApJ*, 164, 111
 Campbell, S. W., & Lattanzio, J. C. 2008, *A&A*, 490, 769
 Carollo, D., Beers, T. C., Bovy, J., et al. 2012, *ApJ*, 744, 195
 Carollo, D., Martell, S. L., Beers, T. C., & Freeman, K. C. 2013, *ApJ*, 769, 87
 Cayrel, R., et al. 2004, *A&A*, 416, 1117
 Christlieb, N., Gustafsson, B., Korn, A. J., et al. 2004, *ApJ*, 603, 708
 Cohen, J. G., Christlieb, N., Thompson, I., et al. 2013, *ApJ*, 778, 56
 Collet, R., Asplund, M., & Trampedach, R. 2007, *A&A*, 469, 687
 Dalton, G., Trager, S., Abrams, D. C., et al. 2016, *Proc. SPIE*, 9908, 99081G
 Dekker, H., D’Odorico, S., Kaufer, A., Delabre, B., & Kotzlowski, H. 2000, *Proc. SPIE*, 4008, 534
 Depagne, E., Hill, V., Spite, M., et al. 2002, *A&A*, 390, 187
 François, P., et al. 2017, in preparation
 Frebel, A., Aoki, W., Christlieb, N., et al. 2005, *Nature*, 434, 871
 Frebel, A., Christlieb, N., Norris, J. E., et al. 2006, *ApJ*, 652, 1585
 Frebel, A., Johnson, J. L., & Bromm, V. 2007, *MNRAS*, 380, L40
 Frebel, A., Collet, R., Eriksson, K., Christlieb, N., & Aoki, W. 2008, *ApJ*, 684, 588-602
 Gaia Collaboration, Brown, A. G. A., Vallenari, A., et al. 2016, *A&A*, 595, A2
 Gallagher, A. J., Caffau, E., Bonifacio, P., et al. 2017, *A&A*, 598, L10
 Gallagher, A. J., Caffau, E., Bonifacio, P., et al. 2016, *A&A*, 593, A48
 González Hernández, J. I., Bonifacio, P., Ludwig, H.-G., et al. 2008, *A&A*, 480, 233
 Gao, S., Liu, C., Zhang, X., et al. 2014, *ApJ*, 788, L37
 Gustafsson, B., Edvardsson, B., Eriksson, K., Graae-Jørgensen, U., Nordlund, Å., & Plez, B. 2008, *A&A* 486, 951
 Hansen, T., Hansen, C. J., Christlieb, N., et al. 2014, *ApJ*, 787, 162
 Hansen, C. J., Nordström, B., Hansen, T. T., et al. 2016, *A&A*, 588, A37

Table 2. Stellar parameters and abundances of C and Li

Star	T_{eff} K	$\log g$ [C's]	ξ Km/s	[Fe/H]	A(C) 1D	A(C) 3D	A(Ca) Ca II-K	A(Li)	EW(Li) pm
SDSS J0140+2344	5848	4.0	1.5	-4.00 ± 0.14	6.33	6.11		1.86	2.2
SDSS J1034+0701	6224	4.0	1.5	-4.01 ± 0.14	6.28	5.96		2.24:	2.8:
SDSS J1035+0641	6262	4.0	1.5	< -5.20	7.16	6.95	1.5	1.90	1.3
SDSS J1247-0341	6332	4.0	1.5	-4.01 ± 0.32	6.64	6.35		2.20:	2.2:
SDSS J1349+1407	6112	4.0	1.5	-3.60 ± 0.12	7.00	6.82		< 0.9	< 0.3
SDSS J1442-0015	5850	4.0	1.5	-4.37 ± 0.16	6.02	5.71		< 1.58	< 1.2
SDSS J1507+0051	6555	4.0	1.5	-3.41 ± 0.20			< 2.19	< 1.6	

Table 3. Abundances relative to hydrogen [X/H] with solar abundances from Lodders et al. (2009) for all elements except Fe and C whose solar abundances are from Caffau et al. (2011a).

El	Sun	J0140+2344	J1034+0701	J1035+0641	J1247-0341	J1349+1407	J1442-0015	J1507+0051
C I	8.50	-2.17	-2.22	-1.33	-1.86	-1.50	-2.48	
Na I	6.30	-4.22				-2.74 ± 0.12		
Mg I	7.54	-3.37 ± 0.02	-3.28 ± 0.10		-3.77 ± 0.23	-2.18 ± 0.11	-4.19 ± 0.05	-3.30 ± 0.13
Al I	6.47	-4.29	-4.27		< -4.23	-3.97	< -4.68	< -4.03
Si I	7.52	-3.91	-4.12		-4.27		-4.53	-3.67
Ca I	6.33	-2.79	-4.17			-3.42 ± 0.16	-4.48	-3.35
Ca II	6.33	-3.66		-4.83	-4.07			-3.05
Sc II	3.10		-3.38			-3.54		
Ti I	4.90						-2.33	-3.04 ± 0.12
Ti II	4.90	-3.75 ± 0.14	-3.84 ± 0.04			-3.22 ± 0.15	-2.44	
Cr I	5.64	-4.17 ± 0.12				-3.73		
Mn I	5.64					-3.87 ± 0.03		
Fe I	7.52	-4.00 ± 0.14	-4.01 ± 0.14	< -5.20	-4.01 ± 0.32	-3.60 ± 0.12	-4.37 ± 0.16	-3.41 ± 0.20
Fe II	7.52					-3.58 ± 0.16		-3.56
Co I	4.92	-3.13 ± 0.34				-2.87		
Ni I	6.23	-3.86 ± 0.12	-3.99			-3.43		
Sr II	2.92	-3.43 ± 0.06						-3.16 ± 0.02

- Hayes, C. R., Majewski, S. R., Shetrone, M., et al. 2017, arXiv:1711.05781
- Hirano, S., Hosokawa, T., Yoshida, N., et al. 2014, ApJ, 781, 60
- Ito, H., Aoki, W., Beers, T. C., et al. 2013, ApJ, 773, 33
- Ivans, I. I., Sneden, C., James, C. R., et al. 2003, ApJ, 592, 906
- Ivans, I. I., Sneden, C., Gallino, R., Cowan, J. J., & Preston, G. W. 2005, ApJ, 627, L145
- Izzard, R. G., Glebbeek, E., Stancliffe, R. J., & Pols, O. R. 2009, A&A, 508, 1359
- Karakas, A. I. 2016, Mem. Soc. Astron. Italiana, 87, 229
- Karakas, A. I. 2010, MNRAS, 403, 1413
- Keller, S. C., Bessell, M. S., Frebel, A., et al. 2014, Nature, 506, 463
- Koch, A., McWilliam, A., Grebel, E. K., Zucker, D. B., & Belokurov, V. 2008, ApJ, 688, L13
- Koch, A., Lind, K., & Rich, R. M. 2011, ApJ, 738, L29
- Kurucz, R. 1993, SYNTHES Spectrum Synthesis Programs and Line Data. Kurucz CD-ROM No. 18. Cambridge, Mass.: Smithsonian Astrophysical Observatory, 1993., 18
- Kurucz, R. L. 2005, Memorie della Società Astronomica Italiana Supplementi, 8, 14
- Lee, Y. S., Beers, T. C., Sivarani, T., et al. 2008, AJ, 136, 2022
- Li, X., Zhao, G., Chen, Y.-Q., & Li, H.-N. 2014, Research in Astronomy and Astrophysics, 14, 1423-143
- Li, H.-N., Zhao, G., Christlieb, N., et al. 2015a, ApJ, 798, 110
- Li, H., Aoki, W., Zhao, G., et al. 2015b, PASJ, 67, 84
- Lodders, K., Plame, H., & Gail, H.-P. 2009, Landolt-Börnstein - Group VI Astronomy and Astrophysics Numerical Data and Functional Relationships in Science and Technology Volume 4B: Solar System. Edited by J.E. Trümper, 2009, 4.4., 44
- Lucatello, S., Gratton, R., Cohen, J. G., et al. 2003, AJ, 125, 875
- Masseron, T., Johnson, J. A., Plez, B., et al. 2010, A&A, 509, A93
- Masseron, T., Johnson, J. A., Lucatello, S., et al. 2012, ApJ, 751, 14
- Matsuno, T., Aoki, W., Beers, T. C., Lee, Y. S., & Honda, S. 2017, AJ, 154, 52
- Moe, M., & Di Stefano, R. 2017, ApJS, 230, 15
- Monaco, L., Villanova, S., Bonifacio, P., et al. 2012, A&A, 539, A157
- Norris, J. E., Ryan, S. G., Beers, T. C., & Deliyannis, C. P. 1997, ApJ, 485, 370
- Norris, J. E., Ryan, S. G., Beers, T. C., Aoki, W., & Ando, H. 2002, ApJ, 569, L107
- Pasquini, L., Koch, A., Smiljanic, R., Bonifacio, P., & Modigliani, A. 2014, A&A, 563, A3
- Placco, V. M., Beers, T. C., Reggiani, H., & Meléndez, J. 2016, ApJ, 829, L24
- Plez, B. 2012, Turbospectrum: Code for spectral synthesis, astrophysics Source Code Library
- Plez, B., & Cohen, J. G. 2005, A&A, 434, 1117
- Plez, B., Cohen, J. G., & Meléndez, J. 2005, From Lithium to Uranium: Elemental Tracers of Early Cosmic Evolution, 228, 267
- Roederer, I. U., Preston, G. W., Thompson, I. B., et al. 2014, AJ, 147, 136
- Sbordone, L. 2005, Memorie della Società Astronomica Italiana Supplementi, 8, 61
- Sbordone, L., Bonifacio, P., Castelli, F., & Kurucz, R. L. 2004, Mem. Soc. Astron. Italiana, 5, 93
- Sbordone, L., et al. 2010, A&A, 522, A26
- Sbordone, L., Caffau, E., Bonifacio, P., Duffau, S., 2013, A&A, submitted
- Sbordone, L., Caffau, E., & Bonifacio, P. 2012, American Institute of Physics Conference Series, 1480, 160
- Sivarani, T., Bonifacio, P., Molero, P., et al. 2004, A&A, 413, 1073
- Sivarani, T., Beers, T. C., Bonifacio, P., et al. 2006, A&A, 459, 125
- Spite, M., Andrievsky, S. M., Spite, F., et al. 2012, A&A, 541, A143
- Spite, M., Caffau, E., Bonifacio, P., et al. 2013, A&A, 552, A107
- Stancliffe, R. J., & Glebbeek, E. 2008, MNRAS, 389, 1828
- Starkenburg, E., Martin, N., Youakim, K., et al. 2017, MNRAS, 471, 2587
- Susmitha Rani, A., Sivarani, T., Beers, T. C., et al. 2016, MNRAS, 458, 2648
- Thompson, I. B., Ivans, I. I., Bisterzo, S., et al. 2008, ApJ, 677, 556

- Wood, P. R. 2011, 9th Pacific Rim Conference on Stellar Astrophysics, 451, 87
Yoon, J., Beers, T. C., Placco, V. M., et al. 2016, *ApJ*, 833, 20
Yong, D., et al. 2013, *ApJ*, 762, 26
Youakim, K., Starkenburg, E., Aguado, D. S., et al. 2017, *MNRAS*, 472, 2963